Development of a consumer-grade scanning platform for fruit thermal and position data collection

Development of a consumer-grade scanning platform for fruit thermal and position data collection

1st Gianmarco Bortolotti
Department of Agricultural and Food Sciences (DISTAL)
University of Bologna
Bologna, Italy
gianmarco.bortolotti@unibo.it

2nd Mirko Piani
Department of Agricultural and Food Sciences (DISTAL)
University of Bologna
Bologna, Italy
mirko.piani2@unibo.it

3rd Dario Mengoli
Department of Electrical, Electronic, and Information Engineering (DEI)
University of Bologna
Bologna, Italy
dario.mengoli2@unibo.it

4th Cristiano Franceschini
Department of Agricultural and Food Sciences (DISTAL)
University of Bologna
Bologna, Italy
cristia.franceschin2@unibo.it

5th Nicolò Omodei
Department of Electrical, Electronic, and Information Engineering (DEI)
University of Bologna
Bologna, Italy
nicolo.omodei@unibo.it

6th Simone Rossi
Department of Electrical, Electronic, and Information Engineering (DEI)
University of Bologna
Bologna, Italy
simone.rossi39@unibo.it

7th Luigi Manfrini
Department of Agricultural and Food Sciences (DISTAL)
University of Bologna
Bologna, Italy
luigi.manfrini@unibo.it

***Abstract*— Climate change and more frequent heatwaves exacerbate the issue of fruit sunburn in orchards. To facilitate fruit temperature dynamics investigation, in relation to fruit sunburn damage occurrence, a low-cost thermal scanning platform, based on depth and thermal consumer-grade cameras, was developed to collect position and temperature fruit information. The platform exploits the Robotic Operating System (ROS) to synchronize data collection from the sensors, the YOLOv5 object detection algorithms to automatically detect fruits to be analyzed, and a Python based pipeline to align images and extract temperature and position information of the fruits (apple and grape cluster). Results referred to a first version of the system shown a high correlation between estimated and actual temperature (r > 0.92) and an acceptable positional error (~ 0.15m). Many improvements of the system are currently on-going to reach the expected performance on a second version of the platform.**

Keywords*— Fruit temperature, fruit Sunburn, sensor fusion, computer vision system, automation

I. INTRODUCTION

Climate change exacerbate issues related to fruit crops production, modifying the typical phenological stage timing, increasing heat and water stresses periods to which plants and growers have to overcome, generally considering site-specific adaptation approaches [1], [2]. Due to the more frequent heatwaves, the risk of sunburn increases as the temperature rises due to excessive solar radiation and thermal stress [3], [4]. This not only compromises the marketability of the produce, thereby reducing growers' incomes, but also entails indirect economic burdens as a result of additional protective measures. Understanding the impact of heatwaves on the incidence and severity of fruit sunburn is a crucial step for protecting crop yields and assuring growers' profitability [5].

Being able to forecast the occurrence of possible fruit sunburn damage based on past, current, and forecasted weather data would be interesting for growers. This would enable the adoption of defense strategies such as kaolin spraying, climate-conditioning irrigation (e.g., over-canopy irrigation) as well as using netting systems to increase shading levels [6].

To reach this objective, fruit temperature dynamics in relation to sunburn occurrence need to be investigated taking in to account many variables such as the fruit species considered, the place and the way they are grown and managed as well as weather and microclimatic data of the surrounding area. Much of this information is easily and quickly attainable, such as weather or microclimatic data (e.g., through weather service or private weather station), fruit species, training system and management (by brief interview to the growers), or pedo-geological information (exploiting online GPS-based-repository). Conversely, the fruit temperature and position information needed for this investigation are collected mainly manually, thus requiring labor, increasing cost, and limiting the numerosity of samples.

To overcome this situation and ease the application of machine learning approaches requiring a wide amount of ground-truth data, automatic data collection of fruit temperature and position is essential. Some studies already report systems able to autonomously collect fruit temperature data later used for investigating fruit sunburn occurrence [7]–[9]. However, a system able to integrate fruit positional information able to map fruit temperature related to its position in the field, possibly in near real-time, has not been released and developed yet.

The goal of the presented study is to develop and test a scanning platform called 'RGB-D/T' based on ready-to-use consumer-grade set of sensors as well as a computer vision system (CVS) and object-detection algorithms [10], [11]. The platform realization objective is to facilitate fruit thermal and

spatial data collection by introducing automation and possibly exploiting autonomous vehicles like the one described in [12].

II. MATERIALS AND METHODS

A. Platform setup

Fig. 1. Left) The 3D printed case holding (a) thermal camera and (b) RGB-D camera. Right) Platform sensors set-up and field data collection.

To implement the RGB-D/T system, consumer-grade sensors were specifically integrated in the setup to investigate possible "low-budget" solutions able to scan the orchards for fruit temperature distribution. A depth (or RGB-D) Intel RealSense D435i camera and a SEEK CompactPro thermal camera were utilized as sensor suite (Fig. 1). In order to firmly hold the cameras during the measurements and maintain their mutual positions, a 3D printed case was created and customized to fit with sensors' shapes.

This was designed to vertically align the center of both the cameras lenses, while keeping the distance between them as reduced as possible, so to favor overlapping in cameras field of view (FoV). The 3D printed case was firmly fixed (with screws) on a wood pole equipped with two bubble levels and mounted on a tripod equipped as well with a bubble level.

Data collection platform consisted of a standard laptop (MSI Katana GF66), exploiting a ROS (Robotic Operating System) workflow. The development of a ROS workflow to collect the data was essential to synchronize the frames from the two sensors. In addition, while the RGB-D camera was supported with a dedicated ROS driver, the SEEK CompactPro thermal camera was not, featuring only an official, but not open source, smartphone application based on Android OS. Thus, exploiting an open-source third-party software development kit (SDK), a custom ROS node was developed allowing both sensors to work simultaneously from the same ROS-Linux based platform (i.e., a laptop in this case).

The ROS workflow allows to generate "*.bag*" files containing synchronized data from both sensors. From these files, it was later possible to extract the same timing synchronized data collected from both the cameras, despite their differences in frame rates.

B. Color and thermal image alignment

Since the two cameras are sensible to different wavelength (visible vs infrared), it was necessary to exploit both spectra to proper align images. For doing that, an alignment panel was made using small heating lightbulbs (n. lights = 30, diameter = 5 mm) mounted 125 mm apart on a wooden board, so to create a chessboard scheme, as already described in [9]. The high temperature and light emission of these bulbs, allowed to

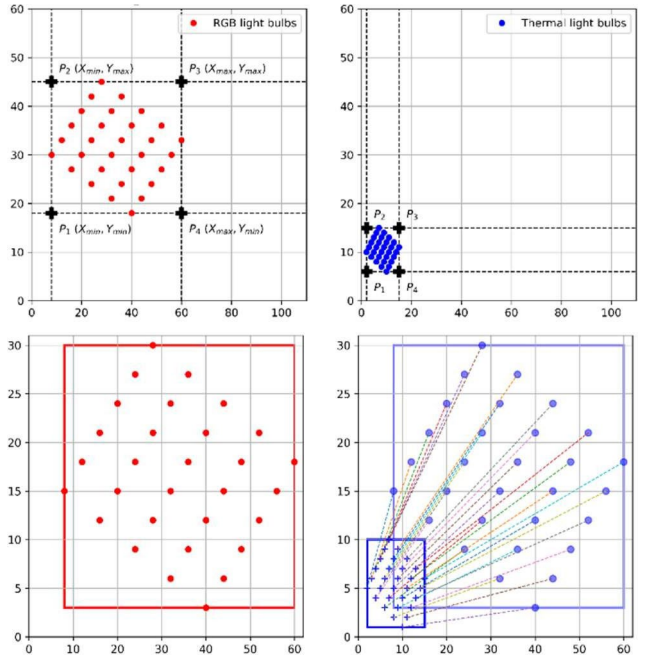

Fig. 2. Top) definition of the smallest area, enclosing all the keypoints for both color (red) and thermal (blue) images; Bottom) Example of thermal-to-RGB projection.

distinguish them from the background both in RGB colors and temperature data. From the images collected using this panel, an alignment process was performed as follows (Fig.2):

1. SimpleBlobDetector function from OpenCV library was used to detect the light bulbs in both RGB and thermal images (after a parameter tuning for each image type).
2. Keypoints' coordinates obtained from the blob detectors were used to determine the corners of the smallest bounding-box enclosing all the keypoints, thus define points *P1, P2, P3, P4* in Fig.2.
3. A scaling factor for both *x* and *y* axis was computed and used to resize the thermal image and align it to the corresponding RGB one by projecting all the pixels collected by the thermal camera.

The mean scaling factor obtained from 18 images was then included in the ROS workflow to align RGB and thermal images during operation.

C. Fruit detection

In order to automate the data extraction instead of exploiting RGB color/thermal filtering as in [7], [8] a 'YOLOv5-m' object detection algorithms was trained to identify fruits. Two models were developed for this purpose: one for apple fruit (mAP = 0.734 and F1-score = 0.74) and one for grape clusters (mAP = 0.973 and F1-score = 0.96) detection. The first model was trained leveraging on a proprietary dataset of 208 tree apple images collected in orchard during 2020-2021 seasons, while the second was trained exploiting an existing grape image WGISD dataset from[13]. These were then applied on the ROS-extracted RGB images, collected with the RGB-D/T system, to identify the fruit pixels in the images and apply the thermal analysis.

D. Thermal calibration of the system

Since the raw-to-Celsius degree thermal conversion equation used by the official Android app for the SEEK thermal camera, is neither open-source nor available for

developers, reverse engineering approach was exploited to get the proper calibration functions and convert raw thermal data obtained through the ROS workflow in Celsius degrees. To achieve this result, the same scenes containing several objects of known temperature were collected using both ROS framework and the Android app. The following steps were performed:

1. Since raw thermal data obtained with the two collecting methods presented a different scale according to common thermal values (e.g., 0-6k vs 0-17k "Raw Thermal Units" (RTU) respectively for the Android app and ROS framework), it was not possible to directly convert ROS collected data to Celsius degrees (°C) and a ROSraw-to-SEEKraw data conversion algorithm was needed to ensure a proper conversion. Conversion coefficients for linear equations were extracted by means of pixel-to-pixel regression analysis. Despite the not strong correlation ($r = 0.60$), the RMSE (4%) was acceptable and the ending results after the ROSraw-to-SEEKraw conversion presented a suitable data resolution and a proper representation (not preserved when using other different approaches).
2. After this step, relationship between raw thermal data (in SEEKraw RTU range) and Celsius degrees given by the Android app was investigated. The result was not found to be a linear relationship in the tested temperature range (i.e., -4 to 100°C). By this, three raw thermal data domains, having a linear relation, were defined (< 3k, 3k-7k, >7k RTU). While investigating this, it was found that objects temperature readings were notably altered by their distance from the sensors. Because of that, a data collection of the same scene was done with an object-to-camera distance variable from 0.5 to 3.0 m considering 0.5 m steps. As a result, a discrete SEEKraw-to-°C correction equations for each of the thermal domain and distance combination was computed.
3. At each distance, objects of different known temperatures were measured, and the error compared with the reference was computed. A calibration equation for each of minimum, maximum, and mean temperature of the scene was computed by interpolating errors recorded at the six distances, so to enable temperature-distance correction at all distances between the collected range.

E. Fruit temperature extraction process

1. The fruit temperature extraction algorithm starts by applying the YOLOv5 object detection model on the RGB image. The algorithm defines all the possible fruits (detected) from which to extract temperature information. For each analyzed image, the center coordinate, the width, and the height of the bounding box (bbox) for every detected fruit are stored into a dataframe (yoloDF).
2. The ROSraw thermal image is aligned to the RGB one (see step B.) then is clipped at each fruit bbox coordinate, defined in yoloDF, creating an aligned thermal bbox (Tbbox) containing raw thermal information of the fruit.
3. Per each clipped Tbbox, a filtering step is applied to check if the detected fruit (on the RGB image) falls in the thermal camera FoV: if >40% of the Tbbox are zero (unavailable) values, then the Tbbox is discarded, otherwise the process continues.
4. The remaining Tbbox-es are analyzed for their thermal information and a percentile filtering step was developed to extract the temperature of the warmer spot/area of the fruit bbox, considering the purpose of the project, related to sunburn damage occurrence. At this phase, all the pixel values with temperature below the 70th percentile are discarded and not considered in the further steps. This filtering is essential also for removing thermal information not pertinent to the fruit (i.e., background, small areas with overlapping leaf, etc.).
5. After this step only raw thermal data of the 70th – 100th percentile remain, and the following steps occurs:
    a. Firstly, raw thermal data are converted in their official SEEK app values range (see D.1).
    b. According to the obtained thermal values and shooting distance, the optimal raw-to-Celsius conversion function is applied (see D.2-3).
    c. At last, the minimum, mean and maximum temperature of the spot are computed and corrected for the distance error (see D.3). Since remaining fruit temperatures will always be near or above environmental temperature, these values are corrected using only max and mean temperature related correction coefficients obtained in *D.3*.

F. 3D Fruit positioning

To map fruit position, the depth information coming from the RGB-D sensor (i.e., depth map) was exploited. Before extracting positional information, a filtering step was applied to discard invalid values (i.e., zeros) present in the depth image due to geometrical/computational constraints or noise occurring in the data collection. Similarly to fruit thermal data extraction, YOLOv5 models were used to detect fruit on the RGB image and clip the aligned depth map for the detected area object (Dbbox). To remove depth information related to the background around the fruit, a distance occurrence filtering step was applied to Dbbox: low occurrence (< 10-15%) distances were discarded, while others depth data were maintained. The most represented (i.e., with highest occurrence) depth information, was then considered as the "mean fruit distance" (Z coordinate of the fruit, using the camera frame) since this should be the one better representing the fruit. Then, the X and Y coordinates of the fruit center were considered to be equal to the detected fruit bbox center.

To re-compute fruit coordinates with respect to the trunk, the position of this was needed. Trunk was detected in the image using a dedicated YOLOv5 model, then the mean trunk distance (Z) was computed as presented for fruits. Since trunk was considered as the origin at its ground level, instead of using its X and Y "center" as done for the fruit, only X bbox center coordinate was considered as X-trunk coordinate, while Y-trunk coordinate was extracted as the Y lowest value in the bbox (since this is the closest point to the ground in the trunk bbox). Once knowing both the fruit and the trunk coordinates in the same measure unit (X and Y in pixels, Z in millimeters) and from the same coordinate system origin (the RGB-D camera), it was possible to compute the fruit position relative to the trunk. This was done by simply subtracting from each fruit coordinates the correspondent trunk coordinates. Applying this technique on all the detected fruits of an image allowed to obtain a fruit distribution map of the whole plant.

The X and Y pixel coordinates were finally converted in millimeters, to obtain real world values. This was done exploiting a trigonometric approach accounting for mean object distance and camera's FoV as reported in [10] and [14].

G. System evaluation

A Field data collection to evaluate preliminary system performances was done. This consisted of a brief video recording (3 sec) of a single tree, using the ROS framework from both the cameras. For apple trees trained as "thin" spindle, the tripod was positioned in front of the tree trunk at 2.80 m distance perpendicular to the tree-row plane (Z), with cameras parallel to the tree-row plane (X). Considering the possible tree height, after the tripod positioning, two height recordings occurred: one at 1.40 m (h1) and one at 2.50 m (h2) from the ground (Y) thus to be able to collect as much thermal data as possible considering the reduced FoVs (32° x 32°) of the thermal camera compared to the RGB ones (69° x 42°). The system was levelled thanks to the three level bubbles present on the tripod. The system positioning and the height and distance selected, managed to frame one entire tree in width and having a minimum reliable thermal analysis resolution of 11.2 x 11.2 mm (i.e., analysis of a 2 x 2 pixels matrix). With this approach data were collected, on 6 trees presenting fruits close to maturity stage with red epidermis color (cv Gala) and 6 trees loading fruits at earlier development stages with green skin color (cv Fuji).

For grape data collection, a similar setup using the same X, Y, Z dimension and approach were utilized. In this case the tripod was placed in front of the middle of the plant canopy, not using the trunk as central referring point, at 2.30 m distance, so to frame one entire vine in width and height, having a minimum reliable analysis resolution of 9.6 x 9.6 mm (i.e., 2 x 2 pixels matrix). With this approach, after veraison, 16 single vine (trained as VSP spur pruned cordon - cv Sangiovese) recordings were collected, presenting different levels of defoliation or fruit occlusion.

III. Results and Discussion

A. RGB-thermal alignement evaluation

The performance assessment consisted into comparing the projected positions of *P1, P2, P3, P4* thermal points with the actual coordinates directly extracted from the RGB images (N=18 * 4 points). The evaluation pointed out a RMSE / mean error of ±9.17 / +4.5 pixels and ±4.17 / +0.17 pixels, on x-axis and y-axis respectively. Considering the dimensions of target objects (apples and grape clusters), this error guarantees that most of the thermal data obtained, is related to target objects, despite inaccuracies due to alignment errors.

B. Fruit temperature extraction

The evaluation of the temperature estimation performances was made throughout a comparison with a factory calibrated handheld thermal camera (HTI) based on field data collection where target reference objects for minimum (refrigerated container), "mean-ambient" (operators' hand) and maximum (one highly exposed fruit) temperature were included. The temperature was then extracted through the developed pipeline – see E) exploiting manual labeling of the target object – and compared to HTI collected temperatures. Collected temperatures for this trial presented high correlation between the two sensors (r = 0.93 – 0.98).

Further data analysis is currently ongoing to have a more reliable evaluation related mostly on fruit temperatures, but preliminary results on apple fruits measured through HTI handled thermal camera as reference (N=12) showed an RMSE / mean error ranging from ±1.38 / -0.95 °C to ±6.72 / +6.59 °C, with best results for extraction and correction of average temperature of the fruit. Preliminary results of the system on grape clusters detection and temperature extraction pointed out an RMSE / mean error ranging from ±3.43 / -0.96 °C to ±10.36 / -9.79 °C, for single cluster temperature measured with thermocouples (N=16) with the lowest errors occurring when considering maximum fruit temperature extraction and correction.

These results are quite encouraging, particularly considering the strong correlation with reference temperature. In addition, the low mean errors presented when dealing with maximum-mean fruit temperature corrections (±1.38 and ±3.43 °C respectively for apple and grape) point a high potentiality of the system for reliable max fruit temperature estimation. Despite that the system is still not accurate as other presented solutions [7], [8] for in field data collection.

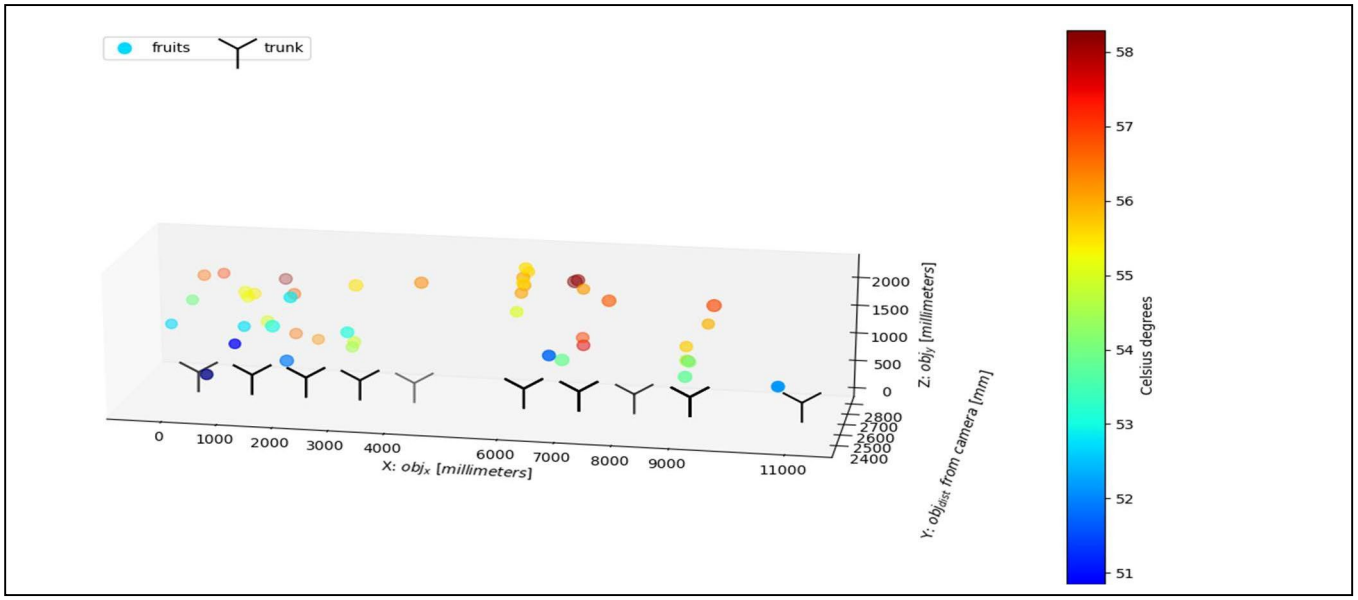

Fig. 3. Graphical output of the developed platform: representation of the 3D fruit temperature distribution of an apple orchard row.

C. 3D Fruit positioning

The evaluation of the 3D fruit positioning of the system and process performances in obtaining positional information is currently ongoing. Very preliminary results based on few fruits from images collected in field (N<20) pointed out that the system seems to present an RMSE of ± 0.15 m approx. in positioning the fruit center with respect to the reference fruit. Further analysis both in laboratory and in field conditions are currently ongoing to obtain more robust results, but considering the purpose of the system, in positioning the fruit on the tree, an error of 0.15 m seems acceptable when dealing with plant dimensions (i.e., meters); infact, a fruit wrong placed 15 cm apart from where it actually is hanging still an acceptable representation of its position on a vine or an apple tree.

In Fig. 3 is shown a graphical representation of the RGB-D/T system final output of the system, where both thermal and positional information of fruit of different trees are depicted. Despite the obtained results, further improvements are still needed to increase the performance of the system, in fact, in the same figure, automatically detected fruits temperatures present a range of 51 - 58°C, that is above of the known temperature thresholds for sunburn occurrence in apple [3]; despite this, only for few fruits sunburn damage occurred. This, together with the fruit temperature extraction performances previously presented, highlight that the system still needs for improvement to correctly estimate fruit temperature in field. Regarding this, new temperature-to-distance corrections, and increased dataset for raw-to-°C thermal data conversion equations are under development and datasets for thermal and 3D positioning evaluation (currently under analysis) will be further enlarged. In addition, new fruit detection models will be applied to increase detection performances and identify only those most exposed fruit, since these are the most informative for investigating sunburn related fruit temperature dynamics; with the purpose to extract information properly related to the fruit surface only also the utilization of and improved circle detection algorithm will be implemented in the fruit detection pipeline[11]. Moreover, as can be seen in Fig. 3, trunk positions are currently expressed as a distance (in mm) from the beginning of the orchard row in which data collection occurred. In a new version of the RGB-D/T platform, a GPS receiver will be included to georeferencing plants (and consequentially fruits), this in order to enable the use of an automated vehicle for data harvesting [15] as well as GIS analysis. In this newer version, fruit sizing and tracking [16] functionality will be implemented to test in-field real-time orchard scanning.

IV. Conclusion

The presented study described a first prototype of a low-cost RGB-D/T scanning platform (software available at[17], [18]) for in field fruit temperature and position data collection. The purpose of this platform was to ease (by automate) data collection enabling orchard mapping and support the utilization of machine learning approaches, requiring wide amount of data, to investigate fruit temperature dynamics related to sunburn occurrence. The results presented refers to a first version of the system and can be summarized in an already acceptable performance level for the purpose of the system, with thermal and position error of ±1.38 °C and ± 0.15 m in best case scenario. Despite this, as highlighted in the discussion, further improvement are still needed to increase both system precision and accuracy during field measurements.

Furthermore, as anticipated, the authors are currently working on a second version of the platform that will be mounted on an autonomous vehicle to actually test its capability in automatically mapping fruit position, temperature and (probably) size in near real-time.

Acknowledgment

This work was supported by the SHEET European project. The project SHEET (Sunburn and heat prediction in canopies for evolving a warning tech solution) is part of the ERA-NET co-funded ICT-AGRI-FOOD, with funding provided by national sources (Italian Ministry of the University and Research) and co-funding by the European Union's Horizon 2020 research and innovation program, Grant Agreement number 862665.

References

[1] J. M. Cabezas, M. Ruiz-Ramos, M. A. Soriano, C. Gabaldón-Leal, C. Santos, and I. J. Lorite, "Identifying adaptation strategies to climate change for Mediterranean olive orchards using impact response surfaces," *Agric Syst*, vol. 185, p. 102937, Nov. 2020, doi: 10.1016/j.agsy.2020.102937.

[2] I. J. Lorite *et al.*, "The role of phenology in the climate change impacts and adaptation strategies for tree crops: a case study on almond orchards in Southern Europe," *Agric For Meteorol*, vol. 294, p. 108142, Nov. 2020, doi: 10.1016/j.agrformet.2020.108142.

[3] L. E. Schrader, J. Zhang, and W. K. Duplaga, "Two Types of Sunburn in Apple Caused by High Fruit Surface (Peel) Temperature," *Plant Health Prog*, pp. 1–6, 2001, doi: 10.1094/PHP-2001-1004-01-RS.

[4] L.-S. Chen, P. Li, and L. Cheng, "Effects of high temperature coupled with high light on the balance between photooxidation and photoprotection in the sun-exposed peel of apple," *Planta*, vol. 228, no. 5, pp. 745–756, Oct. 2008, doi: 10.1007/s00425-008-0776-3.

[5] D. Zanotelli, L. Montagnani, C. Andreotti, and M. Tagliavini, "Water and carbon fluxes in an apple orchard during heat waves," *European Journal of Agronomy*, vol. 134, p. 126460, Mar. 2022, doi: 10.1016/j.eja.2022.126460.

[6] A. Boini *et al.*, "Gala apple production benefits from high shading levels and water limitation, under exclusion netting," *Sci Hortic*, vol. 310, p. 111756, Feb. 2023, doi: 10.1016/j.scienta.2022.111756.

[7] A. K. Chandel, L. R. Khot, Y. Osroosh, and T. R. Peters, "Thermal-RGB imager derived in-field apple surface temperature estimates for sunburn management," *Agric For Meteorol*, vol. 253–254, pp. 132–140, May 2018, doi: 10.1016/j.agrformet.2018.02.013.

[8] R. Ranjan, L. R. Khot, R. T. Peters, M. R. Salazar-Gutierrez, and G. Shi, "In-field crop physiology sensing aided real-time apple fruit surface temperature monitoring for sunburn prediction," *Comput Electron Agric*, vol. 175, p. 105558, Aug. 2020, doi: 10.1016/j.compag.2020.105558.

[9] N. Tsoulias, S. Jörissen, and A. Nüchter, "An approach for monitoring temperature on fruit surface by means of thermal point cloud," *MethodsX*, vol. 9, Jan. 2022, doi: 10.1016/j.mex.2022.101712.

[10] D. Mengoli, G. Bortolotti, M. Piani, and L. Manfrini, "On-line real-time fruit size estimation using a depth-camera sensor," in *2022 IEEE Workshop on Metrology for Agriculture and Forestry (MetroAgriFor)*, IEEE, Nov. 2022, pp. 86–90. doi: 10.1109/MetroAgriFor55389.2022.9964960.

[11] G. Bortolotti, M. Gullino, M. Piani, D. Mengoli, and L. Manfrini, “67. Apple fruit sizing through low-cost depth camera and neural network application,” in *Precision agriculture ’23*, The Netherlands: Wageningen Academic Publishers, Jul. 2023, pp. 531–537. doi: 10.3920/978-90-8686-947-3_67.

[12] R. Tazzari, D. Mengoli, and L. Marconi, “Design Concept and Modelling of a Tracked UGV for Orchard Precision Agriculture,” in *2020 IEEE International Workshop on Metrology for Agriculture and Forestry (MetroAgriFor)*, IEEE, Nov. 2020, pp. 207–212. doi: 10.1109/MetroAgriFor50201.2020.9277577.

[13] T. T. Santos, L. L. de Souza, A. A. dos Santos, and S. Avila, “Grape detection, segmentation, and tracking using deep neural networks and three-dimensional association,” *Comput Electron Agric*, vol. 170, p. 105247, Mar. 2020, doi: 10.1016/j.compag.2020.105247.

[14] G. Bortolotti, D. Mengoli, M. Piani, L. C. Grappadelli, and L. Manfrini, “A computer vision system for in-field quality evaluation: preliminary results on peach fruit,” in *2022 IEEE Workshop on Metrology for Agriculture and Forestry (MetroAgriFor)*, IEEE, Nov. 2022, pp. 180–185. doi: 10.1109/MetroAgriFor55389.2022.9965022.

[15] D. Mengoli, R. Tazzari, and L. Marconi, “Autonomous Robotic Platform for Precision Orchard Management: Architecture and Software Perspective,” in *2020 IEEE International Workshop on Metrology for Agriculture and Forestry (MetroAgriFor)*, IEEE, Nov. 2020, pp. 303–308. doi: 10.1109/MetroAgriFor50201.2020.9277555.

[16] D. Mengoli *et al.*, “57. An online fruit counting application in apple orchards,” in *Precision agriculture ’23*, The Netherlands: Wageningen Academic Publishers, Jul. 2023, pp. 459–465. doi: 10.3920/978-90-8686-947-3_57.

[17] G. Bortolotti, M. Piani, D. Mengoli, N. Omodei, S. Rossi, and L. Manfrini, “ECOPOM/SHEET_RGBD-T_system_v_2022: SHEET_RGBD- T_system_by_ECOPOM.” Zenodo, Feb. 2023. doi: 10.5281/zenodo.7627740.

[18] M. Piani, G. Bortolotti, D. Mengoli, N. Omodei, S. Rossi, and L. Manfrini, “SHEET_RGBD-T_system_v_2022.” Feb. 2023. doi: https://doi.org/10.5281/zenodo.7541753